Journal of Neuroradiology 46 (2019) 268–275

Available online at ScienceDirect www.sciencedirect.com

Elsevier Masson France EM|consulte www.em-consulte.com

Review

Review of synthetic MRI in pediatric brains: Basic principle of MR quantification, its features, clinical applications, and limitations

Christina Andica [a], Akifumi Hagiwara [a,b,*], Masaaki Hori [a], Koji Kamagata [a], Saori Koshino [a,b], Tomoko Maekawa [a,b], Michimasa Suzuki [a], Hirokazu Fujiwara [c], Mitsuru Ikeno [d], Toshiaki Shimizu [d], Hiroharu Suzuki [e], Hidenori Sugano [e], Hajime Arai [e], Shigeki Aoki [a]

[a] Department of Radiology, Juntendo University Graduate School of Medicine, 2-1-1, Hongo, Bunkyo-ku, Tokyo, 113-8421, Japan
[b] Department of Radiology, Graduate School of Medicine, The University of Tokyo, 7-3-1, Hongo, Bunkyo-ku, Tokyo, 113-0033, Japan
[c] Department of Radiology, Keio University School of Medicine, 35, Shinanomachi, Shinjuku-ku, Tokyo, 160-8583, Japan
[d] Department of Pediatrics, Juntendo University School of Medicine, 2-1-1, Hongo, Bunkyo-ku, Tokyo, 113-8421, Japan
[e] Department of Neurosurgery, Juntendo University School of Medicine, 2-1-1, Hongo, Bunkyo-ku, Tokyo, 113-8421, Japan

ARTICLE INFO

Article history:
Available online 7 March 2019

Keywords:
Pediatric brain
Brain development
Quantitative MRI
Synthetic MRI
Automatic Brain tissue volumetry
Myelin measurement

ABSTRACT

Quantitative magnetic resonance imaging (MRI) with multislice, multi-echo, and multi-delay acquisition enables simultaneous quantification of R_1 and R_2 relaxation rates, proton density, and the B_1 field in a single acquisition, and requires only about 6 minutes for full-head coverage. Using dedicated SyMRI software, radiologists can generate any contrast-weighted image by manipulating the acquisition parameters, including repetition time, echo time, and inversion time. Moreover, automatic brain tissue segmentation, volumetry, and myelin measurement can also be performed. Using the SyMRI approach, a shorter scan time, an objective examination, and personalized MR imaging parameters can be obtained in daily clinical pediatric imaging. Here we summarize and review the use of SyMRI in imaging of the pediatric brain, including the basic principles of MR quantification along with its features, clinical applications, and limitations.

Introduction

Magnetic resonance imaging (MRI) is now widely used to evaluate the development and pathologies of the pediatric brain [1,2]. However, practical and technical challenges have limited the use of MR examinations in daily practice. First, relatively long scanning times can be an obstacle, especially for infants and young children [1,2]. Second, conventional MR images are interpreted qualitatively by comparing the signal intensities of tissues with surrounding areas. Therefore, signal intensities cannot be used for comparison with normal reference values or for follow-up studies [3]. Third, signal intensities on conventional MR images are affected by the type of scanner or sequences used, differing coil sensitivities, and B_1 field inhomogeneities [4].

However, quantitative MRI provides absolute values for tissue properties, such as R1 and R2 relaxation rates (the inverses of T1 and T2 relaxation times, respectively), and proton density (PD) [5–7]. In pediatric imaging, quantitative information may enable us to chart developmental trajectories or identify brain pathologies, to assess the degree of change in disease severity, and to monitor the course of therapy in an objective manner [8,9]. Moreover, dependence on MR scanner hardware and parameter settings can be minimized [7,10].

MR quantification method using the QRAPMASTER (quantification of relaxation times and proton density by multiecho acquisition of a saturation-recovery using turbo spin-echo readout) pulse sequence enables quantification of R1, R2, PD, and the B1 field in a single acquisition in only about 6 minutes for full-head coverage

Abbreviations: BPF, brain parenchymal fraction; BPV, brain parenchymal volume; CSF, cerebrospinal fluid; DIR, double inversion recovery; FLAIR, fluid-attenuated inversion recovery; GM, gray matter; Gd, gadolinium; V_{EPW}, excess parenchymal water partial volume; ICV, intracranial volume; MRI, magnetic resonance imaging; MERS, mild encephalopathy with a reversible splenial lesion; MS, multiple sclerosis; V_{MY}, myelin partial volume; NoN, non-WM/GM/CSF; PD, proton density; PSIR, phase-sensitive inversion recovery; QRAPMASTER, quantification of relaxation times and proton density by multiecho acquisition of a saturation-recovery using turbo spin-echo readout; STIR, short T1 inversion recovery; SWS, Sturge-Weber syndrome; TE, echo time; TI, inversion time; TR, repetition time; WM, white matter.

* Corresponding author at: Department of Radiology, Juntendo University Graduate School of Medicine, 2-1-1, Hongo, Bunkyo-ku, Tokyo, 113-8421, Japan.
E-mail address: a-hagiwara@juntendo.ac.jp (A. Hagiwara).

https://doi.org/10.1016/j.neurad.2019.02.005
0150-9861/

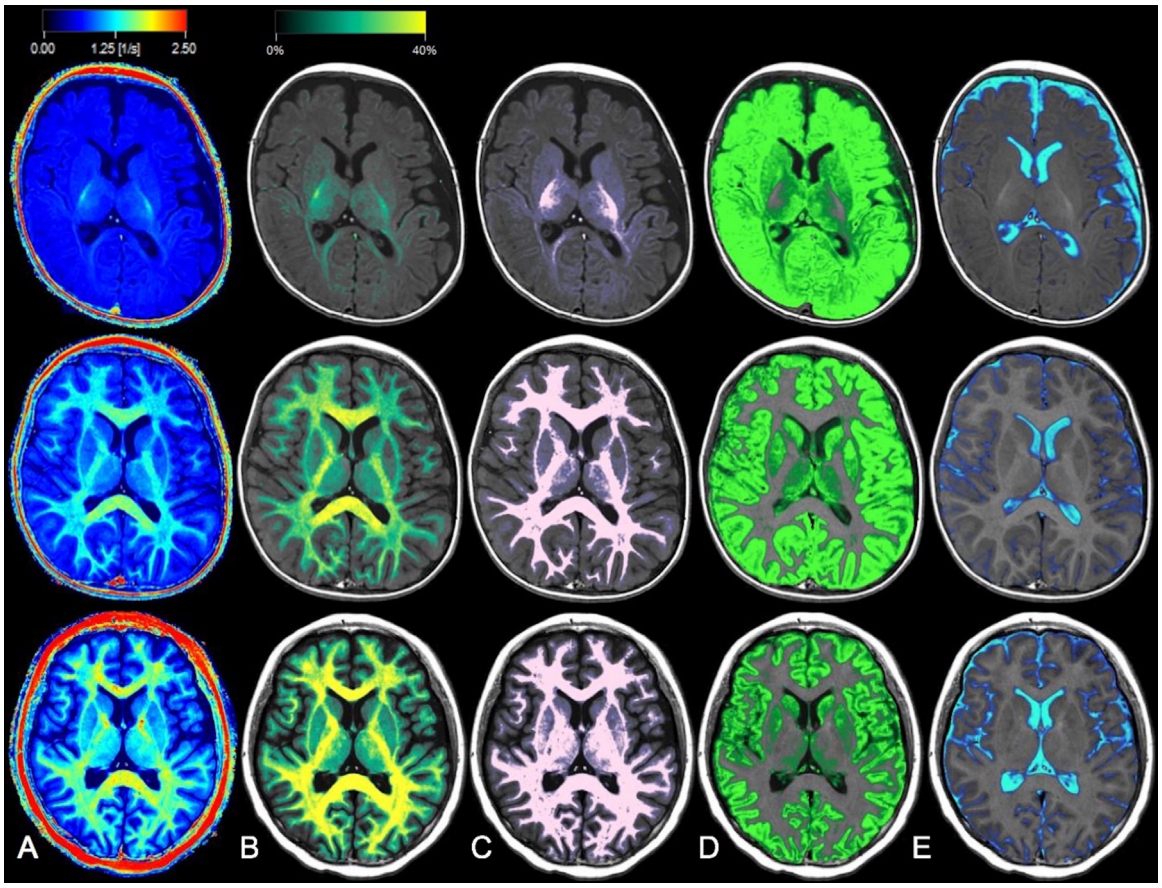

Fig. 1. The brains of a 3-month-old male infant (first row), a 2-year-old boy (second row), and a 13-year-old girl (third row). SyMRI quantitative maps [only R1 map (shown on a scale 0–2.5 s^{-1}) is shown (A)], myelin partial volume map (shown on a scale 0–40%) (B), WM segmentation (C), GM segmentation (D), and CSF segmentation (E) can be used to evaluate development of the brain. However, in young children, WM and GM segmentation is suboptimal because the unmyelinated WM is assigned as GM, which is a limitation of the currently implemented algorithm.

with good accuracy and reproducibility even across different vendors [7,10,11]. Based on the quantitative values, tailored contrast-weighted images can be synthesized and automatic brain tissue volumetry, and myelin measurement can be performed using post-processing SyMRI (SyntheticMR, Linköping, Sweden) software.

Use of SyMRI may overcome the limitations of conventional MRI in pediatric brain imaging. This review article provides an overview of SyMRI, including the basic principles of the QRAPMASTER pulse sequence along with its features, clinical applications, and limitations.

Basic principles of MR quantification

The QRAPMASTER sequence includes two phases that are repeated for complete quantification of tissue parameters. In the first phase, a slice-selective saturation pulse (θ) acts on a slice *n*, followed by spoiling of the signal ("saturation"). In the second phase, a slice-selective turbo spin-echo acquisition of another slice m ("acquisition"), consisting of multiple echoes that are acquired to measure the R2, is performed [7,10]. The echo times and echo spacing can be freely chosen to accommodate any dynamic range for the measurement of R2 [7,10].

By shifting the order of the slices *n* and *m* in relation to each other, the desired delay time between saturation and acquisition of a particular slice can be set. By using different delay times, the R1 after a saturation pulse is retrieved from multiple scans. The number of scans and the delay times can be freely chosen, therefore, the dynamic range of R_1 can also be set as desired [7]. Further, the starting position of the R1 relaxation curve will be a function of the B1 field. Based on R1, R2, and B1, the unsaturated magnetization (M0) that is proportional to the PD can be extracted [10].

QRAPMASTER is using a combination of multiple echo times and delay times; for example, 2 echo times and 4 delay times are used to generate 8 complex images [10]. The quantification of R1, R2, and PD is performed simultaneously, and the resulting maps are intrinsically co-registered.

Features of SyMRI

Measurements of quantitative values

In the first few years of life, the development of the brain is marked by progressive myelination of WM and growth of new synapses in the GM [12,13]. Quantitative relaxometry studies have observed prolonged relaxation times for neonates, followed by a steep decline in both T1 and T2 values, especially during the first 2 years of life; subsequently, a slower decrease extends into the third year, at which time the relaxation parameters approach adult values [12]. Thus, changes in T1 and T2 values provide a sensitive index for assessment of normal brain maturation that reflects the alterations in water content and distribution (Fig. 1) [14]. Hagmann et al. [15] showed a prolonged T2 for cerebral WM in preterm infants imaged at term-equivalent age when compared with T2 in term-control infants. Moreover, Abernethy et al. [16] also showed increased T2 in preterm children with minor motor impairment.

The quantitative values, i.e., R1, R2, and PD, can be obtained by drawing ROIs on the synthetic quantitative maps. Thus, quantitative MRI allows an objective comparison between brains based on

the absolute values of relaxation behavior and water content [7,10]. Previous study has demonstrated the age-dependent changes of T1, T2, and PD values obtained using synthetic MRI in 89 healthy children, from neonate to adolescent [19]. They also provided age-specific regional reference values that could be used as objective tools for the assessment of normal/abnormal brain development [19].

Synthetic contrast-weighted images

In pediatric imaging, patient-to-patient-based imaging parameters are necessary to optimize the brain-tissue contrast because:

- heavily T2WI is needed in infants younger than 12 months of age because the water content in the brain is higher than that in older children and adults; and;
- the contrast between GM and WM and between normal and pathologic tissues is poor [20].

However, adjusting the parameters of conventional MRI to each patient is difficult in daily clinical practice.

Using the approach of synthetic MRI, radiologists can manipulate TE, TR, and TI, retrospectively and "synthesize" any contrast image without the need for additional scanning time [7]. The signal intensity, S, can be calculated using known R1, R2, and PD values for each voxel with the following equation [7]:

$$S \propto PD\,[1 - \exp\,(-R1TR)]\,exp(-R2TE)$$

Inversion-recovery images, such as fluid-attenuated inversion recovery (FLAIR) and short T1 inversion recovery (STIR) images [7,10] can also be synthesized by adding TI, according to

$$S \propto PD[1 - 2\exp\,(R_1TI) + \exp\,(-R_1TR)]exp(-R_2\,TE)$$

Furthermore, a double inversion recovery (DIR) [10] can be synthesized using 2 TIs (TI_1 and TI_2), according to

$$S \propto PD[1 - 2\exp\,(-R_1TI_1) + 2\exp\,(-R_1TI_2) - exp(-R_1TR)]exp(-R_2TE)$$

The clinical feasibility of synthetic MR images in the pediatric brain has been evaluated and compared with conventional MR images. Overall, image quality for conventional and synthetic T1WI and T2WI were comparable and can be used in daily clinical practice [3,4,24–26]. Moreover, the pattern of myelination based on patient age was estimated similarly between the conventional and synthetic approaches [3].

Motion artifact is one of the main concerns in pediatric brain imaging, especially with longer acquisition time, while the use of sedation may increase the risk of morbidity or complications [1]. Previous studies compared the artifacts in synthetic T1WI, T2WI, and FLAIR to conventional T1WI, T2WI, and FLAIR in pediatric brains, including motion artifacts. The results demonstrated that overall motion was mild in synthetic images and not significantly different from conventional images [3,26]. So far, synthetic MRI has been solely performed with Cartesian sampling, while radial sampling may reduce motion artifacts. However, caution is warranted when applying radial sampling to synthetic MRI, because of the possible change in acquired signals and larger aliasing effects than Cartesian sampling [27].

Brain tissue segmentation and volumetry

Longitudinal studies of brain volumetry can be a good objective indicator for detecting developmental disorders. For example, the whole brain and GM volumes in children with cerebral palsy were significantly reduced in comparison with those in controls [28]. Meanwhile, brain volume overgrowth has been observed in children with autism spectrum disorder [29]. Assessment of brain tissue volumetry may also be advantageous in the evaluation of some brain pathologies, such as follow-up of ventricular size in patients with hydrocephalus or in the monitoring of severity of atrophy in those with leukodystrophies [4].

Automatic brain tissue segmentation by SyMRI was developed based on a predefined quantitative value for each type of brain tissue, which forms a cluster in three-dimensional space, i.e., the R1-R2-PD space [30]. A lookup grid is then created to relate tissue partial volumes to the R1-R2-PD space, so that the partial volume error can be reduced [30]. The lookup grid then translates the acquired MR quantitative values into WM, GM, or cerebrospinal fluid (CSF) tissue volume fractions, and the voxels outside the lookup grid are considered as Non-WM/GM/CSF (NoN). Brain parenchymal volume (BPV) as the sum of WM, GM, and NoN, intracranial volume (ICV) as the sum of BPV and CSF, and brain parenchymal fraction (BPF) as the ratio of BPV to ICV can also be calculated automatically.

Automatic SyMRI brain tissue volumetry has been shown to be robust and to have a shorter post-processing time than manual segmentation and other types of automatic MR-based brain volumetry software [10,31–33]. Further, SyMRI brain tissue volumetry has also shown good repeatability with different in-plane resolutions and geometries [30,34].

McAllister et al. [35] proposed that age-associated intracranial tissue volumes derived from SyMRI had good agreement with known child brain volume growth chart. However, there are some limitations in very young subjects because of suboptimal GM and WM segmentations where unmyelinated WM tends to be assigned as GM (Fig. 1). Even though SyMRI volumetry has been extensively studied in adults [30–33,36–38], segmentation may not be accurate in children when using fully automated image processing methods that are not adapted to normalize and segment the pediatric brain.

Measurement of myelin

Assessment of myelination has become a key factor in the evaluation of neurologic development [39,40]. At the present time, brain myelination is evaluated based on changes in the pattern of signal intensity on T1WI and T2WI and considers neuroanatomic distribution. However, precise visual evaluation is difficult, especially in the presence of developmental variability or if the observer lacks experience [41]. An objective assessment is required for accurate quantification of myelination [40,42].

Warntjes et al. [43] proposed a model in which each acquisition voxel is assumed to be composed of four partial volumes: myelin partial volume (V_{MY}); cellular partial volume; free water partial volume; and excess parenchymal water partial volume (V_{EPW}), where each partial volume has its own R1, R2, and PD [43]. The estimation of V_{MY} in this model also considers magnetization exchange between the myelin water component trapped between the myelin sheaths and the surrounding intracellular and extracellular water [10,43].

Warntjes et al. [44] showed the validity of this myelin measurement model by demonstrating a good correlation with brain slices stained using Luxol Fast Blue [44]. Hagiwara et al. [45] have also shown that V_{MY} correlates well with magnetization transfer imaging, which is considered to be one of the criterion standards for myelin imaging. In the normal pediatric population, myelin measured by SyMRI was well fitted to a maturation curve [19,35,46].

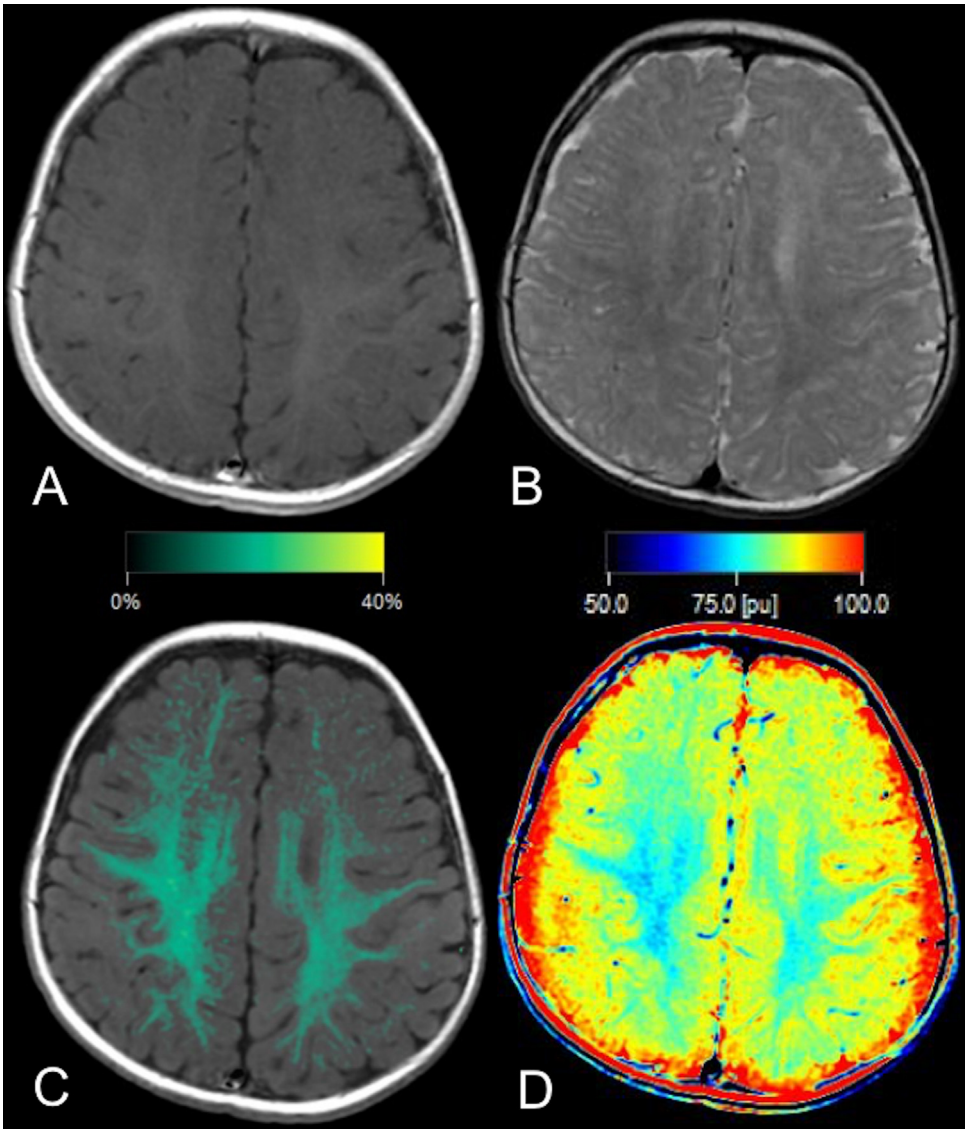

Fig. 2. Images from a 7-month-old male infant with right facial angiomatosis and suspected to have Sturge-Weber syndrome. No significant finding, including of leptomeningeal angiomatosis, is shown on synthetic T1WI or T2WI before or after administration of gadolinium (Gd). Here we show post-Gd synthetic T1WI (A) and pre-Gd synthetic T2WI (B). However, a myelin partial volume map (shown on a scale 0–40%) overlaid on a synthetic T1WI (C) shows increased a myelin partial volume in the cerebral WM on the right side (ipsilateral) when compared with the left hemisphere with decreased PD on a PD map (shown on a scale 50–100 pu) (D). The total volume of myelin is 9.32 mL in the right cerebral hemisphere and 7.86 mL in the left hemisphere. These findings may reflect accelerated hypermyelination.

Clinical applications

Sturge–Weber syndrome

Sturge–Weber syndrome (SWS) is characterized by facial and leptomeningeal angiomatosis [47,48]. Previous case reports have demonstrated the utility of SyMRI in the diagnosis of SWS [21,22,49].

Dural enhancement in SWS is rarely reported, although angiomatous changes in the dura mater have been demonstrated in SWS pathologically [22,48]. Gadolinium (Gd)-enhanced synthetic DIR images, which suppress signals of bone marrow fat and CSF, can be used to show dural enhancement [22].

Accelerated myelination has been shown to be one of the possible causes of abnormal T2 hypointensity in the ipsilateral WM [47]. Quantitative SyMRI maps are useful for showing shorter T1, T2, and lower PD in the affected area, reflecting the myelination process (Fig. 2) [20,21]. Synthetic T2WI with longer TR and TE can be used to optimize the contrast and show the hypointensity more clearly [21], while synthetic DIR can be used to suppress the non-myelinated area and CSF so that the myelinated area can be highlighted [21]. Further, V_{MY} map and myelin volumetry can provide objective values for evaluation of accelerated myelination by comparing the right and left hemispheres (Fig. 2).

Meningitis

The clinical presentation of meningitis in infancy is usually nonspecific and CSF analysis is less useful [23]. The sensitivity of Gd enhanced-FLAIR images has been reported to be higher than Gd-enhanced T1WI, but Gd enhanced-FLAIR is not routinely performed [50]. In SyMRI, Gd-enhanced synthetic FLAIR can be readily synthesized after image acquisition. Gd-enhanced synthetic DIR, which suppresses signals of CSF and fat, may also be useful for showing subtle meningeal enhancement [23].

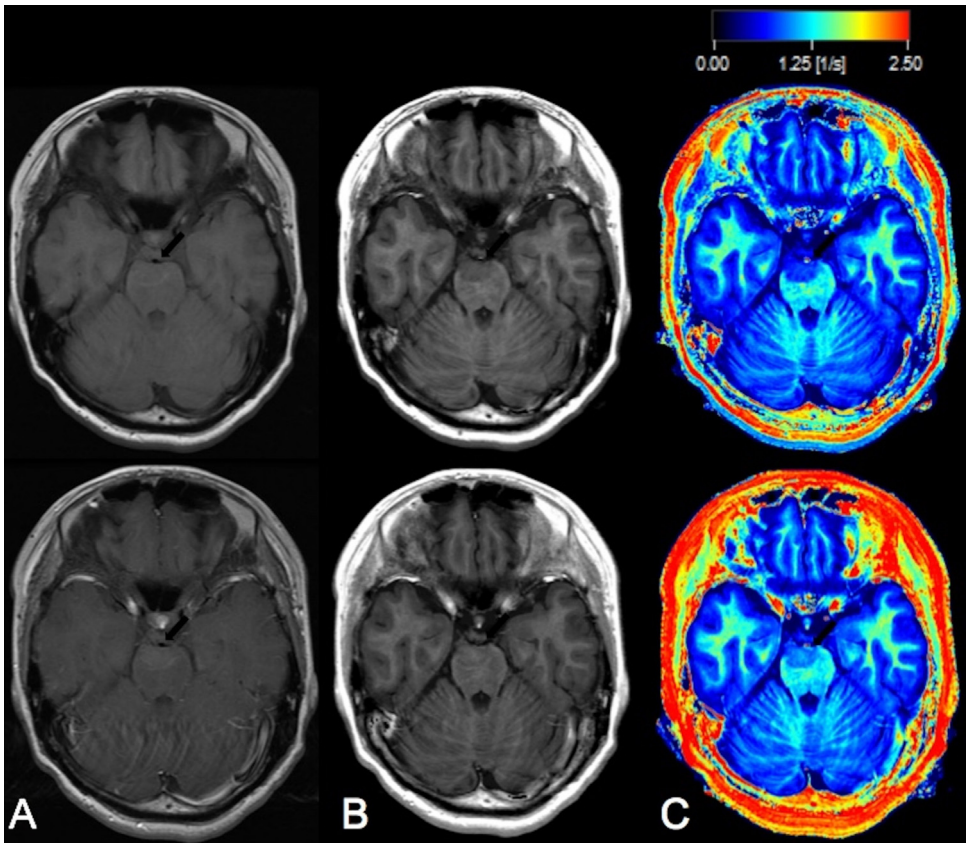

Fig. 3. A case of brainstem glioma (arrow) scanned with conventional and synthetic MRI before (first row) and after (second row) administration of gadolinium. A pre-gadolinium synthetic T1WI (B) shows the hypointense lesion in the pons more clearly than a pre-gadolinium conventional T1WI (A). Post-gadolinium conventional and synthetic T1WI shows only a subtle enhancement. The R1 map (shown on a scale 0–2.5 s^{-1}) (C) shows a higher R1 on the post-gadolinium image (1.03 s^{-1}) in comparison with the pre-gadolinium image (0.79 s^{-1}), reflecting accumulation of gadolinium in the lesion. The quantitative R1 value might be used as an objective assessment not only for diagnosis but also for follow-up studies.

Multiple Sclerosis

Pediatric multiple sclerosis (MS) (with onset before the age of 18 years) accounts for up to 3%–5% of all MS cases [51–53]. MS in children is more aggressive and has a higher relapse rate that MS in adults, and tends to be associated with development of cognitive dysfunction [53,54].

Synthetic MR images enable detection of more MS plaques than conventional MRI [36,55] and use of synthetic DIR and PSIR images may be useful for detection of intra-cortical or mixed WM-GM lesions [55]. Vargberg et al. [33] showed that SyMRI volumetry is a valid and reproducible method for determining BPF in MS. In line with adult MS, the BPF has been shown to be significantly lower in pediatric MS, and the decrease is mostly accounted for by loss of GM [53].

Contrast-enhancing plaques are markers of active inflammation in MS [56]. Blystad et al. [56] showed that enhancing plaques had significantly higher R1 and R2 and lower PD values than non-enhancing plaques. These quantitative values can be a predictor for Gd enhancement. Further, V_{MY} and V_{EPW} have also been found to be sensitive biomarkers of the MS disease process [57,58].

Brainstem Glioma

Brainstem glioma accounts for 10%–20% of all intracranial tumors in children, and 75%–85% of these tumors are classified as diffuse midline glioma [59,60]. Most diffuse brainstem gliomas do not enhance or only show minimal heterogeneous enhancement [61]. However, assessment of enhancement can be used to predict the prognosis of brainstem glioma and to evaluate the response to therapy or a recurrence [59].

As discussed previously, quantitative values acquired by SyMRI enable us to show Gd enhancement, revealing an increased R1 in enhanced tissues [56]. Therefore, SyMRI might be used to evaluate enhancement objectively and for comparisons in follow-up studies (Fig. 3).

Further, quantitative values might also be used in the evaluation of brain tumors, i.e., to discriminate differences between glioblastomas and metastases [17]. Quantitative values can also demonstrate the internal structure of the tumor when compared with normal regions, i.e., a very short T1 in a tumor with lipid content, a long T1 and T2 in cysts and areas of necrosis, a short T1 and T2 in hemorrhage, and low PD in areas of calcification [18].

Mild Encephalopathy with a Reversible Splenial Lesion

Mild encephalopathy with a reversible splenial lesion is characterized by a symmetric lesion in the splenium of the corpus callosum with high-signal intensity on T2WI and FLAIR and iso or low signal intensity on T1WI, with corresponding restriction of diffusion and no contrast enhancement [62]. It has been postulated that intramyelinic edema might be the cause of this entity [63].

This lesion can be shown more clearly using synthetic DIR images than with synthetic T1WI and T2WI, as shown in Fig. 4. In this figure, the V_{MY} map shows decreased myelin in the lesion with a lower R1 and R2 and a higher PD on the quantitative maps, indicating increased water content. This observation may support the 'intramyelinic edema' theory. Note that the SyMRI V_{MY} map

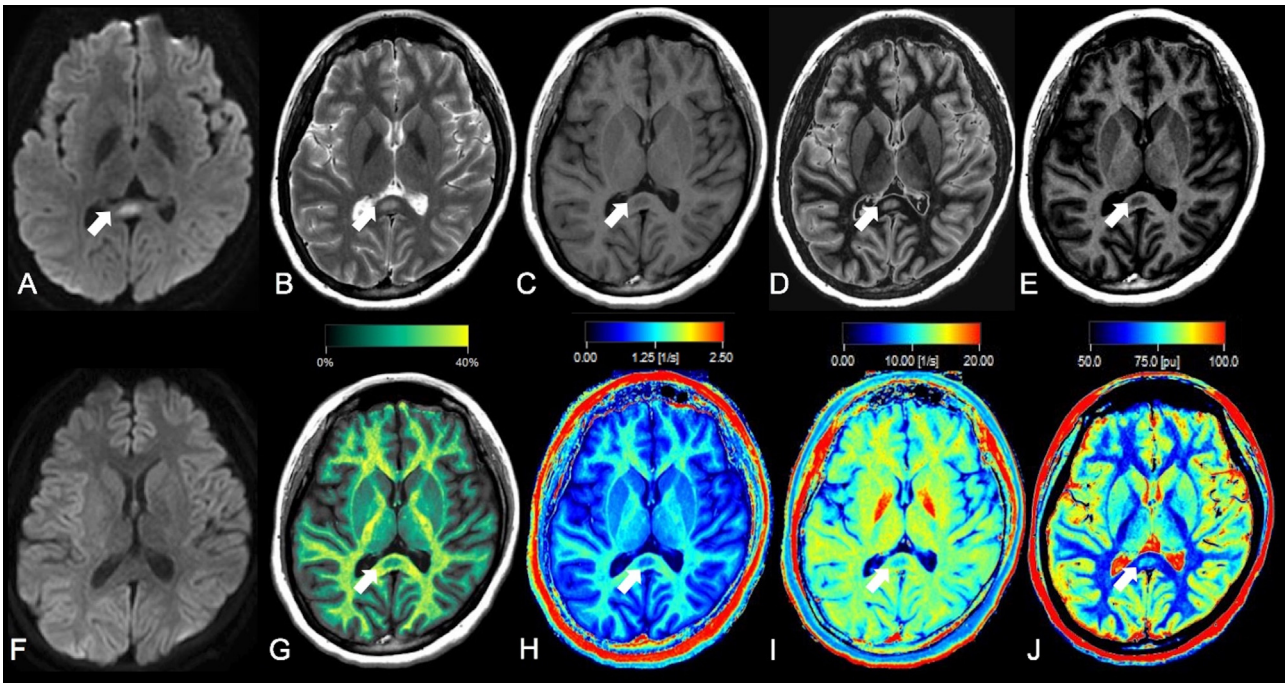

Fig. 4. A lesion (arrow) that is hyperintense on DWI (A) and T2WI (B) and hypointense on T1WI (C) is seen in the splenium of the corpus callosum. Here the lesion is seen more clearly on DIR with WM-CSF suppression (D) and GM-CSF suppression (E). The lesion had resolved completely on the follow-up DWI scan (F) acquired 10 days after the first scan, supporting a diagnosis of MERS. Further, on the initial scan, the myelin content of the lesion was shown to be decreased on the myelin partial volume map (G) with a higher water content shown by the lower R1 and R2, and a higher PD on the R1 (shown on a scale 0–2.5 s^{-1}) (H), R2 (shown on a scale 0–20 s^{-1}) (I), and PD (shown on a scale 50–100 pu) (J) maps, respectively. These results might support the 'intramyelinic edema' theory of MERS. MERS, mild encephalopathy with reversible splenial lesion.

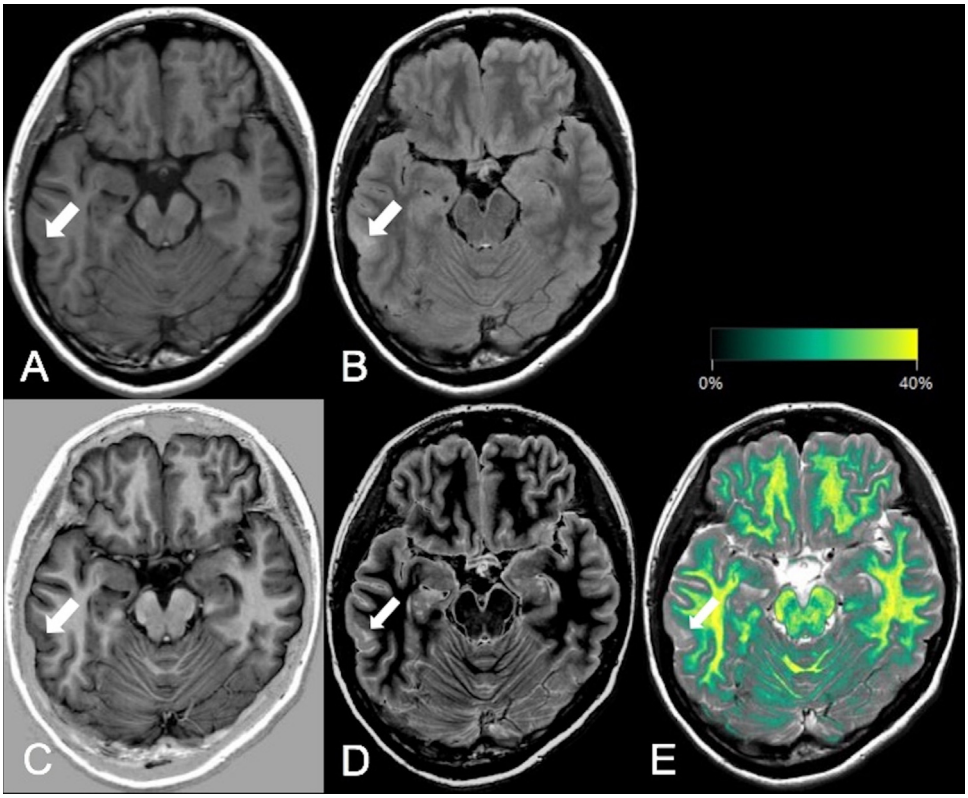

Fig. 5. A subcortical tuber (arrow) that was hypointense on synthetic T1WI (A) and hyperintense on synthetic T2WI seen in the right temporal lobe (B). The lesion is seen more clearly on synthetic phase-sensitive inversion recovery (C) and double inversion recovery (D) with CSF and WM suppressed images. Loss of myelin is evident in this lesion on the myelin partial volume map (shown on a scale 0–40%) overlaid on the synthetic T2WI (E).

was developed based on the fixed R_2 value of myelin [43], and any change in the quantitative values might affect the calculation of myelin.

Tuberous Sclerosis

Tuberous sclerosis is a phakomatosis that frequently affects children and young adults [64]. Cortical or subcortical tubers have been reported in 82%–100% of patients with tuberous sclerosis and are thought to be related to the neurologic manifestations of the disease. Histologic studies have shown that the tubers are hypomyelinated hamartomas [65]. In line with MS, detection of the tubers can be improved by using synthetic DIR and PSIR (Fig. 5). Further, a myelin partial volume map overlaid on the synthetic T2WI enabled us to show loss of myelin within these tubers (Fig. 5).

Limitations of SyMRI

Synthetic FLAIR images have inferior image quality (lower contrast-to-noise ratio) when compared with conventional FLAIR images [3,4,53,66]. Further, the interface of the brain parenchyma and CSF is hyperintense on synthetic FLAIR images, possibly because of partial volume effects [10]. This artifact might be misinterpreted as brain pathology, such as subarachnoid hemorrhage or a cortical MS lesion, so acquisition of additional conventional FLAIR images may be necessary. However, mistakes could be avoided if the images are read cautiously.

Further, Kerleroux et al. [26] showed that phase encoding and fluid pulsation artifacts were more common in synthetic T2WI when compared with conventional T2WI. However, they noted that the phase encoding artifact was easily recognizable and should not be confounded with pathological condition [26]. But, fluid pulsation artifacts might disturb the evaluation of lower brain areas, such as brain stem or cerebral peduncles. Additional conventional images might be beneficial when the clinical symptoms indicate potential pathologies of these structures [26].

Conclusions

A quantitative approach to pediatric brain imaging provides an objective evaluation of the developing brain and its pathologies. The QRAPMASTER pulse sequence enables acquisition of R1, R2, and PD in a single acquisition in a clinically acceptable period of time. Reconstruction of various contrast-weighted images, automatic brain tissue volumetry, and measurement of myelin can be performed retrospectively using dedicated post-processing SyMRI software. Overall, the synthetic images are of a quality comparable with that of conventional MR images and seem to be useful for diagnosis of brain pathologies. Further, SyMRI brain tissue volumetry and myelin measurement demonstrated good agreement with the curve for brain growth. However, some limitations, such as the inferior quality of FLAIR images, and phase encoding and fluid pulsation artifacts, should be noted, and further studies of this technique in patients with various brain diseases are needed.

Disclosure of interest

The authors declare that they have no competing interest.

Funding sources

This work was supported by the Japan Society for the Promotion of Science (JSPS) KAKENHI (grant number 16K19852); by a JSPS Grant-in-Aid for Scientific Research on Innovative Areas, resource and technical support platforms for promoting research 'Advanced Bioimaging Support' (grant number JP16H06280); by the Japan Radiological Society and Bayer Yakuhin (KJ-08); and by the Impulsing Paradigm Change through Disruptive Technologies (ImPACT) Program of the Council for Science, Technology and Innovation (Cabinet Office, Government of Japan).

Acknowledgments

We are grateful to Dr. Takayuki Kon for providing us with relevant clinical information.

References

[1] Bhargava R, Hahn G, Hirsch W, Kim MJ, Mentzel HJ, Olsen OE, et al. Contrast-enhanced magnetic resonance imaging in pediatric patients: review and recommendations for current practice. Magn Reson Insights 2013;6:95–111, http://dx.doi.org/10.4137/MRI.S12561.
[2] Dean 3rd DC, Dirks H, O'Muircheartaigh J, Walker L, Jerskey BA, Lehman K, et al. Pediatric neuroimaging using magnetic resonance imaging during non-sedated sleep. Pediatr Radiol 2014;44(1):64–72, http://dx.doi.org/10.1007/s00247-013-2752-8.
[3] Betts AM, Leach JL, Jones BV, Zhang B, Serai S. Brain imaging with synthetic MR in children: clinical quality assessment. Neuroradiology 2016;58(10):1017–26, http://dx.doi.org/10.1007/s00234-016-1723-9.
[4] West H, Leach JL, Jones BV, Care M, Radhakrishnan R, Merrow AC, et al. Clinical validation of synthetic brain MRI in children: initial experience. Neuroradiology 2017;59(1):43–50, http://dx.doi.org/10.1007/s00234-016-1765-z.
[5] Deoni SC, Peters TM, Rutt BK. High-resolution T1 and T2 mapping of the brain in a clinically acceptable time with DESPOT1 and DESPOT2. Magn Reson Med 2005;53(1):237–41, http://dx.doi.org/10.1002/mrm.20314.
[6] Neeb H, Zilles K, Shah NJ. A new method for fast quantitative mapping of absolute water content in vivo. Neuroimage 2006;31(3):1156–68, http://dx.doi.org/10.1016/j.neuroimage.2005.12.063.
[7] Warntjes JB, Leinhard OD, West J, Lundberg P. Rapid magnetic resonance quantification on the brain: Optimization for clinical usage. Magn Reson Med 2008;60(2):320–9, http://dx.doi.org/10.1002/mrm.21635.
[8] Sled JG, Nossin-Manor R. Quantitative MRI for studying neonatal brain development. Neuroradiology 2013;55(Suppl 2):97–104, http://dx.doi.org/10.1007/s00234-013-1235-9.
[9] Rosenkrantz AB, Mendiratta-Lala M, Bartholmai BJ, Ganeshan D, Abramson RG, Burton KR, et al. Clinical utility of quantitative imaging. Acad Radiol 2015;22(1):33–49, http://dx.doi.org/10.1016/j.acra.2014.08.011.
[10] Hagiwara A, Warntjes M, Hori M, Andica C, Nakazawa M, Kumamaru KK, et al. SyMRI of the brain: rapid quantification of relaxation rates and proton density, with synthetic MRI, automatic brain segmentation, and myelin measurement. Invest Radiol 2017;52(10):647–57, http://dx.doi.org/10.1097/RLI.0000000000000365.
[11] Hagiwara A, Hori M, Cohen-Adad J, Nakazawa M, Suzuki Y, Kasahara A, et al. Linearity, bias, intrascanner repeatability, and interscanner reproducibility of quantitative multidynamic multiecho sequence for rapid simultaneous relaxometry at 3 T: a validation study with a standardized phantom and healthy controls. Invest Radiol 2018 [Epub ahead of print].
[12] Holland BA, Haas DK, Norman D, Brant-Zawadzki M, Newton TH. MRI of normal brain maturation. AJNR Am J Neuroradiol 1986;7(2):201–8.
[13] Knickmeyer RC, Gouttard S, Kang C, Evans D, Wilber K, Smith JK, et al. A structural MRI study of human brain development from birth to 2 years. J Neurosci 2008;28(47):12176–82, http://dx.doi.org/10.1523/JNEUROSCI.3479-08.2008.
[14] Bultmann E, Spineli LM, Gohner F, Hartmann H, Lanfermann H. Age-related T2 relaxation times at 3 Tesla as a biomarker of infratentorial brain maturation. Childs Nerv Syst 2017, http://dx.doi.org/10.1007/s00381-017-3561-4.
[15] Hagmann CF, De Vita E, Bainbridge A, Gunny R, Kapetanakis AB, Chong WK, et al. T2 at MR imaging is an objective quantitative measure of cerebral white matter signal intensity abnormality in preterm infants at term-equivalent age. Radiology 2009;252(1):209–17, http://dx.doi.org/10.1148/radiol.2522080589.
[16] Abernethy LJ, Klafkowski G, Foulder-Hughes L, Cooke RW. Magnetic resonance imaging and T2 relaxometry of cerebral white matter and hippocampus in children born preterm. Pediatr Res 2003;54(6):868–74, http://dx.doi.org/10.1203/01.PDR.0000091285.84577.4E.
[17] Badve C, Yu A, Dastmalchian S, Rogers M, Ma D, Jiang Y, et al. MR fingerprinting of adult brain tumors: initial experience. AJNR Am J Neuroradiol 2017;38(3):492–9, http://dx.doi.org/10.3174/ajnr.A5035.
[18] Peterman SB, Steiner RE, Bydder GM. Magnetic resonance imaging of intracranial tumors in children and adolescents. AJNR Am J Neuroradiol 1984;5(6):703–9.
[19] Lee SM, Choi YH, You SK, Lee WK, Kim WH, Kim HJ, et al. Age-related changes in tissue value properties in children: simultaneous quantification of relaxation times and proton density using synthetic magnetic resonance imaging. Invest Radiol 2018;53(4):236–45, http://dx.doi.org/10.1097/RLI.0000000000000435.
[20] Barkovich A. Pediatric neuroimaging. Philadelphia: Lippincott Williams & Wilkins; 2011.
[21] Andica C, Hagiwara A, Nakazawa M, Tsuruta K, Takano N, Hori M, et al. The advantage of synthetic MRI for the visualization of early white mat-

ter change in an infant with sturge-weber syndrome. Magn Reson Med Sci 2016;15(4):347–8, http://dx.doi.org/10.2463/mrms.ci.2015-0164.
[22] Hagiwara A, Nakazawa M, Andica C, Tsuruta K, Takano N, Hori M, et al. Dural enhancement in a patient with sturge-weber syndrome revealed by double inversion recovery contrast using synthetic MRI. Magn Reson Med Sci 2016;15(2):151–2, http://dx.doi.org/10.2463/mrms.ci.2015-0066.
[23] Andica C, Hagiwara A, Nakazawa M, Kumamaru KK, Hori M, Ikeno M, et al. Synthetic MR imaging in the diagnosis of bacterial meningitis. Magn Reson Med Sci 2017;16(2):91–2, http://dx.doi.org/10.2463/mrms.ci.2016-0082.
[24] Lee SM, Choi YH, Cheon JE, Kim IO, Cho SH, Kim WH, et al. Image quality at synthetic brain magnetic resonance imaging in children. Pediatr Radiol 2017, http://dx.doi.org/10.1007/s00247-017-3913-y.
[25] Tanenbaum LN, Tsiouris AJ, Johnson AN, Naidich TP, DeLano MC, Melhem ER, et al. Synthetic MRI for clinical neuroimaging: results of the magnetic resonance image compilation (MAGiC) prospective, multicenter, multireader trial. AJNR Am J Neuroradiol 2017;38(6):1103–10, http://dx.doi.org/10.3174/ajnr.A5227.
[26] Kerleroux B, Kober T, Hilbert T, Serru M, Philippe J, Sirinelli D, et al. Clinical equivalence assessment of T2 synthesized pediatric brain magnetic resonance imaging. J Neuroradiol 2018, http://dx.doi.org/10.1016/j.neurad.2018.04.003.
[27] Larson PZ, Gurney PT, Nishimura DG. Anisotropic field-of-views in radial imaging. IEEE Trans Med Imaging 2008;27(1):47–57, http://dx.doi.org/10.1109/TMI.2007.902799.
[28] Kulak P, Maciorkowska E, Goscik E. Volumetric magnetic resonance imaging study of brain and cerebellum in children with cerebral palsy. Biomed Res Int 2016;2016:5961928, http://dx.doi.org/10.1155/2016/5961928.
[29] Hazlett HC, Gu H, Munsell BC, Kim SH, Styner M, Wolff JJ, et al. Early brain development in infants at high risk for autism spectrum disorder. Nature 2017;542(7641):348–51, http://dx.doi.org/10.1038/nature21369.
[30] West J, Warntjes JB, Lundberg P. Novel whole brain segmentation and volume estimation using quantitative MRI. Eur Radiol 2012;22(5):998–1007, http://dx.doi.org/10.1007/s00330-011-2336-7.
[31] Ambarki K, Lindqvist T, Wahlin A, Petterson E, Warntjes MJ, Birgander R, et al. Evaluation of automatic measurement of the intracranial volume based on quantitative MR imaging. AJNR Am J Neuroradiol 2012;33(10):1951–6, http://dx.doi.org/10.3174/ajnr.A3067.
[32] Vagberg M, Ambarki K, Lindqvist T, Birgander R, Svenningsson A. Brain parenchymal fraction in an age-stratified healthy population - determined by MRI using manual segmentation and three automated segmentation methods. J Neuroradiol 2016;43(6):384–91, http://dx.doi.org/10.1016/j.neurad.2016.08.002.
[33] Vagberg M, Lindqvist T, Ambarki K, Warntjes JB, Sundstrom P, Birgander R, et al. Automated determination of brain parenchymal fraction in multiple sclerosis. AJNR Am J Neuroradiol 2013;34(3):498–504, http://dx.doi.org/10.3174/ajnr.A3262.
[34] Andica C, Hagiwara A, Hori M, Nakazawa M, Goto M, Koshino S, et al. Automated brain tissue and myelin volumetry based on quantitative MR imaging with various in-plane resolutions. J Neuroradiol 2018;45(3):164–8, http://dx.doi.org/10.1016/j.neurad.2017.10.002.
[35] McAllister A, Leach J, West H, Jones B, Zhang B, Serai S. Quantitative synthetic MRI in children: normative intracranial tissue segmentation values during development. AJNR Am J Neuroradiol 2017, http://dx.doi.org/10.3174/ajnr.A5398.
[36] Granberg T, Uppman M, Hashim F, Cananau C, Nordin LE, Shams S, et al. Clinical feasibility of synthetic MRI in multiple sclerosis: a diagnostic and volumetric validation study. AJNR Am J Neuroradiol 2016;37(6):1023–9, http://dx.doi.org/10.3174/ajnr.A4665.
[37] Virhammar J, Warntjes M, Laurell K, Larsson EM. Quantitative MRI for rapid and user-independent monitoring of intracranial csf volume in hydrocephalus. AJNR Am J Neuroradiol 2016;37(5):797–801, http://dx.doi.org/10.3174/ajnr.A4627.
[38] West J, Blystad I, Engstrom M, Warntjes JB, Lundberg P. Application of quantitative MRI for brain tissue segmentation at 1.5 T and 3.0 T field strengths. PLoS One 2013;8(9):e74795, http://dx.doi.org/10.1371/journal.pone.0074795.
[39] van der Knaap MS, Valk J, Bakker CJ, Schooneveld M, Faber JA, Willemse J, et al. Myelination as an expression of the functional maturity of the brain. Dev Med Child Neurol 1991;33(10):849–57.
[40] Ono J, Kodaka R, Imai K, Itagaki Y, Tanaka J, Inui K, et al. Evaluation of myelination by means of the T2 value on magnetic resonance imaging. Brain Dev 1993;15(6):433–8.
[41] Welker KM, Patton A. Assessment of normal myelination with magnetic resonance imaging. Semin Neurol 2012;32(1):15–28, http://dx.doi.org/10.1055/s-0032-1306382.
[42] Paus T, Collins DL, Evans AC, Leonard G, Pike B, Zijdenbos A. Maturation of white matter in the human brain: a review of magnetic resonance studies. Brain Res Bull 2001;54(3):255–66.
[43] Warntjes M, Engstrom M, Tisell A, Lundberg P. Modeling the presence of myelin and edema in the brain based on multi-parametric quantitative MRI. Front Neurol 2016;7:16, http://dx.doi.org/10.3389/fneur.2016.00016.
[44] Warntjes JBM, Persson A, Berge J, Zech W. Myelin detection using rapid quantitative MR imaging correlated to macroscopically registered luxol fast blue-stained brain specimens. AJNR Am J Neuroradiol 2017;38(6):1096–102, http://dx.doi.org/10.3174/ajnr.A5168.
[45] Hagiwara A, Hori M, Warntjes M, Aoki S. Myelin measurement: comparison between simultaneous tissue relaxometry, magnetization transfer saturation index, and T1w/T2w ratio methods. Sci Rep 2018;10(1):10554, http://dx.doi.org/10.1038/s41598-018-28852-6.
[46] Kim HG, Moon WJ, Han J, Choi JW. Quantification of myelin in children using multiparametric quantitative MRI: a pilot study. Neuroradiology 2017, http://dx.doi.org/10.1007/s00234-017-1889-9.
[47] Moritani T, Kim J, Sato Y, Bonthius D, Smoker WR. Abnormal hypermyelination in a neonate with Sturge-Weber syndrome demonstrated on diffusion-tensor imaging. J Magn Reson Imaging 2008;27(3):617–20, http://dx.doi.org/10.1002/jmri.21248.
[48] Thomas-Sohl KA, Vaslow DF, Maria BL. Sturge-Weber syndrome: a review. Pediatr Neurol 2004;30(5):303–10, http://dx.doi.org/10.1016/j.pediatrneurol.2003.12.015.
[49] Hagiwara A, Andica C, Hori M, Aoki S. Synthetic MRI showed increased myelin partial volume in the white matter of a patient with Sturge-Weber syndrome. Neuroradiology 2017;59(11):1065–6, http://dx.doi.org/10.1007/s00234-017-1908-x.
[50] Splendiani A, Puglielli E, De Amicis R, Necozione S, Masciocchi C, Gallucci M. Contrast-enhanced FLAIR in the early diagnosis of infectious meningitis. Neuroradiology 2005;47(8):591–8, http://dx.doi.org/10.1007/s00234-005-1383-7.
[51] Boiko A, Vorobeychik G, Paty D, Devonshire V, Sadovnick D. University of British Columbia MSCN. Early onset multiple sclerosis: a longitudinal study. Neurology 2002;59(7):1006–10.
[52] Krupp LB, Banwell B, Tenembaum S. International Pediatric MSSG. Consensus definitions proposed for pediatric multiple sclerosis and related disorders. Neurology 2007;68(16 Suppl 2):S7–12, http://dx.doi.org/10.1212/01.wnl.0000259422.44235.a8.
[53] Yeh EA, Weinstock-Guttman B, Ramanathan M, Ramasamy DP, Willis L, Cox JL, et al. Magnetic resonance imaging characteristics of children and adults with paediatric-onset multiple sclerosis. Brain 2009;132(Pt 12):3392–400, http://dx.doi.org/10.1093/brain/awp278.
[54] Narula S, Hopkins SE, Banwell B. Treatment of pediatric multiple sclerosis. Curr Treat Options Neurol 2015;17(3):336, http://dx.doi.org/10.1007/s11940-014-0336-z.
[55] Hagiwara A, Hori M, Yokoyama K, Takemura MY, Andica C, Tabata T, et al. Synthetic MRI in the detection of multiple sclerosis plaques. AJNR Am J Neuroradiol 2017;38(2):257–63, http://dx.doi.org/10.3174/ajnr.A5012.
[56] Blystad I, Hakansson I, Tisell A, Ernerudh J, Smedby O, Lundberg P, et al. Quantitative MRI for analysis of active multiple sclerosis lesions without gadolinium-based contrast agent. AJNR Am J Neuroradiol 2016;37(1):94–100, http://dx.doi.org/10.3174/ajnr.A4501.
[57] Hagiwara A, Hori M, Yokoyama K, Takemura MY, Andica C, Kumamaru KK, et al. Utility of a multiparametric quantitative mri model that assesses myelin and edema for evaluating plaques, periplaque white matter, and normal-appearing white matter in patients with multiple sclerosis: a feasibility study. AJNR Am J Neuroradiol 2017;38(2):237–42, http://dx.doi.org/10.3174/ajnr.A4977.
[58] Hagiwara A, Hori M, Yokoyama K, Nakazawa M, Ueda R, Horita M, et al. Analysis of white matter damage in patients with multiple sclerosis via a novel in vivo mr method for measuring myelin, axons, and G-ratio. AJNR Am J Neuroradiol 2017, http://dx.doi.org/10.3174/ajnr.A5312.
[59] Plaza MJ, Borja MJ, Altman N, Saigal G. Conventional and advanced MRI features of pediatric intracranial tumors: posterior fossa and suprasellar tumors. AJR Am J Roentgenol 2013;200(5):1115–24, http://dx.doi.org/10.2214/AJR.12.9725.
[60] Aboian MS, Solomon DA, Felton E, Mabray MC, Villanueva-Meyer JE, Mueller S, et al. Imaging characteristics of pediatric diffuse midline gliomas with histone H3 K27M Mutation. AJNR Am J Neuroradiol 2017;38(4):795–800, http://dx.doi.org/10.3174/ajnr.A5076.
[61] Poretti A, Meoded A, Huisman TA. Neuroimaging of pediatric posterior fossa tumors including review of the literature. J Magn Reson Imaging 2012;35(1):32–47, http://dx.doi.org/10.1002/jmri.22722.
[62] Ka A, Britton P, Troedson C, Webster R, Procopis P, Ging J, et al. Mild encephalopathy with reversible splenial lesion: an important differential of encephalitis. Eur J Paediatr Neurol 2015;19(3):377–82, http://dx.doi.org/10.1016/j.ejpn.2015.01.011.
[63] Tada H, Takanashi J, Barkovich AJ, Oba H, Maeda M, Tsukahara H, et al. Clinically mild encephalitis/encephalopathy with a reversible splenial lesion. Neurology 2004;63(10):1854–8.
[64] Baron Y, Barkovich AJ. MR imaging of tuberous sclerosis in neonates and young infants. AJNR Am J Neuroradiol 1999;20(5):907–16.
[65] Gallagher A, Grant EP, Madan N, Jarrett DY, Lyczkowski DA, Thiele EA. MRI findings reveal three different types of tubers in patients with tuberous sclerosis complex. J Neurol 2010;257(8):1373–81, http://dx.doi.org/10.1007/s00415-010-5535-2.
[66] Blystad I, Warntjes JB, Smedby O, Landtblom AM, Lundberg P, Larsson EM. Synthetic MRI of the brain in a clinical setting. Acta Radiol 2012;53(10):1158–63, http://dx.doi.org/10.1258/ar.2012.120195.